Separation Science and Technology
Publication details, including instructions for authors and subscription information:
http://www.informaworld.com/smpp/title~content=t713708471

Mineral Stratification in Magnetohydrostatic Separation

I. Yaniv[a]; Y. Zimmels[a]; I. J. Lin[a]
[a] MINERAL ENGINEERING RESEARCH CENTER, HAIFA, ISRAEL

To cite this Article Yaniv, I. , Zimmels, Y. and Lin, I. J.(1979) 'Mineral Stratification in Magnetohydrostatic Separation', Separation Science and Technology, 14: 4, 261 — 290
To link to this Article: DOI: 10.1080/01496397908057147
URL: http://dx.doi.org/10.1080/01496397908057147

SEPARATION SCIENCE AND TECHNOLOGY, 14(4), pp. 261–290, 1979

Mineral Stratification in Magnetohydrostatic Separation

I. YANIV, Y. ZIMMELS, and I. J. LIN*

MINERAL ENGINEERING RESEARCH CENTER, TECHNION—I.I.T.
HAIFA, ISRAEL

Abstract

The magnetohydrostatic method can be used to separate slightly magnetic or nonmagnetic particles according to differences in their specific gravities and magnetic susceptibilities. The classical approach is to effect stratification prior to separation. This paper discusses some of the significant parameters which bear on the design and pattern of the expected stratification in the separation cell. As the characteristics of the magnetic field, and consequently those of the magnetic forces, are determined by the geometry of the poles, this subject is treated first. In this context a new approach, whereby the range of stratification is extended, using positive as well as negative gradients, is presented. Finally, the effect of the relative size and shape of the particles on stratification is discussed.

INTRODUCTION

Magnetohydrostatic separation is based on the "weighting" or "lightening" of a magnetic liquid which serves as a separation medium by means of an external force exerted by a vertical inhomogeneous magnetic field applied to it. Acting in conjunction with gravity, this force causes a solid particle to rise or fall along the gravity axis until equilibrium is established.

In principle, the technique is analogous to the sink–float method, over which it has the following advantages:

(a) It permits simultaneous separation of several fractions.
(b) By appropriate choice of the magnetic field intensity, upward

*To whom correspondence should be addressed.

expulsion of heavy solids and downward expulsion of light ones can be effected.

(c) The value of the induced apparent specific gravities can be varied continuously with variation of the applied field.

(d) The paramagnetic liquid used as the medium is nonvolatile, nontoxic, and often easier to recycle than the heavy liquids commonly used in the sink–float process. It is also cheaper.

THEORETICAL

General

The magnetic force per unit volume of a particle immersed in a magnetic liquid in a nonhomogeneous magnetic field is given by

$$\mathbf{f}_m = \tfrac{1}{2}(\chi_l - \chi_p)\nabla(H^2) \tag{1}$$

In conjunction with gravity and the magnetic susceptibility of the solid particle taken into consideration, the following balance of forces should be satisfied at equilibrium:

$$\mathbf{F}_m + \mathbf{F}_g = 0 \tag{2}$$

Resorting to the concept of specific gravity, we replace Eq. (2) by

$$\rho_p = \rho_l + \tfrac{1}{2}(\chi_l - \chi_p)\nabla(H^2)\cdot\bar{k} \tag{3}$$

where $\bar{k}$ is a unit vector colinear with gravity.

To determine the apparent density of the magnetic liquid, we must know the following parameters:

(a) $\nabla(H^2)$ as a function of the location in the separation cell.
(b) The magnetic susceptibility of the liquid.
(c) The specific gravity of the liquid.

In what follows, we confine ourselves to parameters related to item (a).

Influence of Pole Configuration

The general geometry of wedge-type and curved poles is shown in Figs. 1 and 2.

Assuming that the magnetic permeability of the poles μ is very large

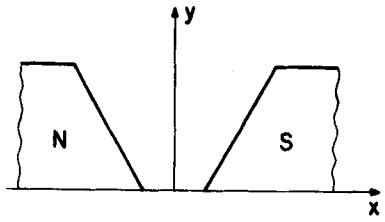

FIG. 1. Geometry of wedge-type pole pieces.

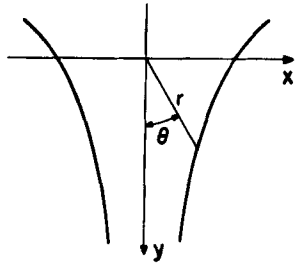

FIG. 2. Geometry of curved pole pieces.

compared with that of the magnetic liquid, we may regard the pole face as an equipotential surface, namely,

$$P = \text{const} \tag{4}$$

The magnetic field is given (*1*) by

$$H = -\nabla P \tag{5}$$

Recalling that the divergence of the field is zero, the Laplace equation is obtained:

$$\nabla^2 P = 0 \tag{6}$$

Equation (6) has two types of solutions which can be used to construct elementary poles. For the wedge-type configuration (*1*):

$$P = A\theta \tag{7}$$

and for the curved configuration:

$$P = Ar^k \sin K\theta \tag{8}$$

Wedge-Type and Curved Configuration

Substituting in Eq. (1) the magnetic fields obtained from Eqs. (7) and (8) by means of (5), we obtain, respectively,

$$\mathbf{f}_m = -\frac{\bar{\chi}_l A^2}{r^3}\mathbf{l}r \tag{9}$$

where

$$\bar{\chi}_l = \chi_l - \chi_p$$

and

$$\mathbf{f}_m = \bar{\chi}_l A^2 k^2 (k-1) r^{(2k-3)}\mathbf{l}r \tag{10}$$

where A is a constant, and $\mathbf{l}r$ is a unit vector colinear with $\mathbf{r}$.

The distribution of the magnetic force per unit volume and of the magnetic field along the y-axis are shown in Figs. 3 and 4.

Influence of Wedge Angle

The influence of the wedge angle on the force distribution is determined as follows (see Fig. 5 for details).

Assuming no *edge effect* (see also the section entitled "Influence of Edge Effects on Magnetic Force and Magnetic Field Distribution") we may write:

$$H_0 h = Hl = \text{const} \tag{11}$$

where $l = x + h$, and H_0 is the magnetic field in the air gap.

Substituting Eq. (11) in (1), we find

$$\mathbf{f}_m = \frac{\bar{\chi}_l H_0^2 h^2}{(x+h)^3}\mathbf{l}y \tag{12}$$

Substituting, as per Fig. 5,

$$h = \frac{d}{2}\cot\theta \tag{13}$$

in Eq. (12), we find the sought relationship (3):

$$\mathbf{f}_m = \frac{\bar{\chi}_l H_0^2 d^2 \cot^2\theta}{4\left(X + \frac{d}{2}\cot\theta\right)^3}\mathbf{l}y \tag{14}$$

Figure 6 shows the force distribution as a function of θ for an aqueous

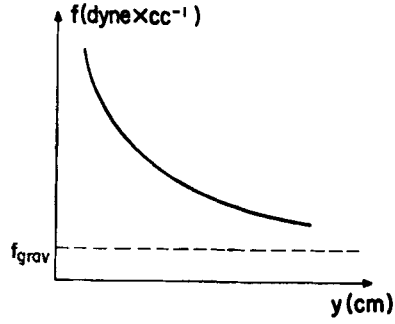

FIG. 3. Magnetic force distribution per unit volume as a function of y for wedge-type pole configuration.

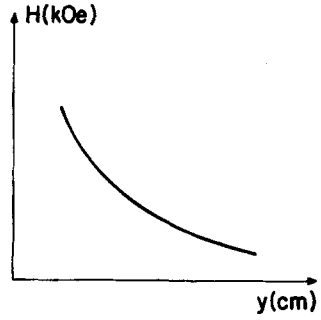

FIG. 4. Magnetic field distribution as a function of y for wedge-type configuration.

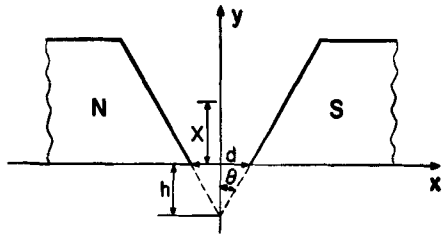

FIG. 5. Geometrical parameters of wedge-type configuration.

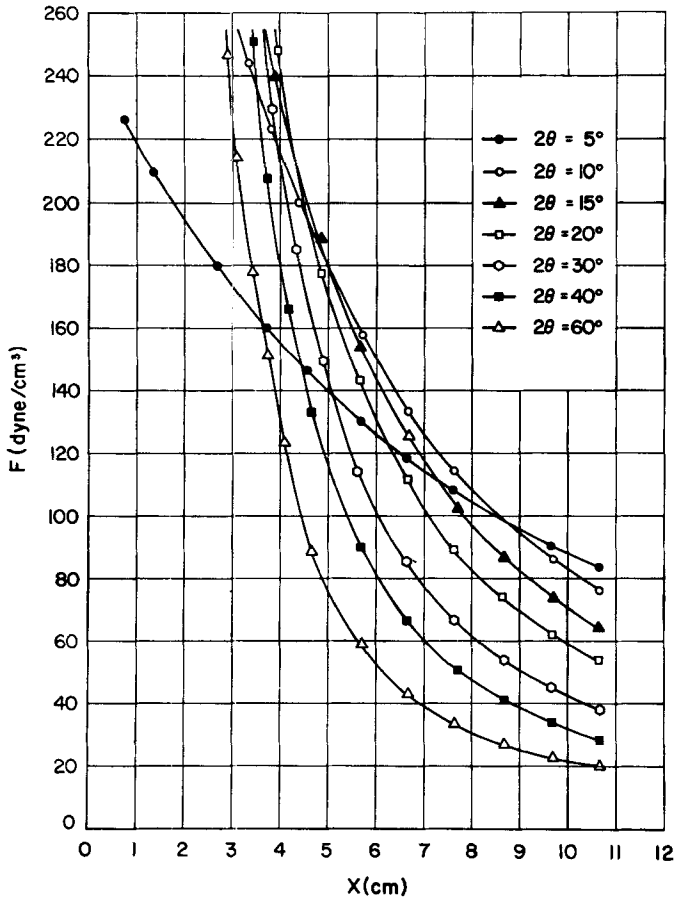

FIG. 6. Influence of wedge angle on magnetic force distribution as a function of location x.

solution of $MnCl_2 \cdot 4H_2O$ with $\chi_l = 50 \times 10^{-6}$ emu/cm^3, an air gap of 2 cm, and an applied field $H_0 = 10$ kOe.

Pole Configuration for Weighting and Lightening the Magnetic Liquid

Weighting. Weighting of the magnetic liquid is effected by the configuration in Fig. 8(b). The apparent density of the liquid is given by

$$\rho_p = \rho_l + \frac{2\bar{\chi}_l H_0^2 d^2 \cot^2 \theta}{g(2y + d \cot \theta)^3} \tag{15}$$

and its distribution along the y-axis is shown in Fig. 7(a).

Lightening. Lightening of the magnetic liquid is effected by the configuration in Fig. 8(a). The apparent density of the liquid is given (*3*) by

$$\rho_p = \rho_l - \frac{2\bar{\chi}_l H_0^2 d^2 \cot^2 \theta}{g(2y + d \cot \theta)^3} \tag{16}$$

and its distribution along the y-axis is shown in Fig. 7(b).

Discontinuous Alternate Lightening and Weighting. Discontinuous alternate lightening and weighting is effected by the configuration in Fig. 8(c). The apparent density is given by Eq. (15) along the positive $(+y)$-direction and by Eq. (16) along the negative $(-y)$-direction. Its distribution along the y-axis is shown in Fig. 7(c).

Continuous Alternate Lightening and Weighting. Continuous alternate lightening and weighting is effected by the configuration in Fig. 8(d). The apparent density can be approximately evaluated by Eq. (15). For $0 \leq y < L/2$ and by Eq. (17) for $L/2 < y \leq L$:

$$\rho_p = \rho_l - \frac{2\bar{\chi}_l H_0^2 d^2 \cot^2 \theta}{(2L + d \cot \theta - 2y)^3}, \tag{17}$$

At $y = L/2$ we have $\rho_p = \rho_l$ as $\nabla H = 0$. The distribution of the apparent density along the y-axis is shown in Fig. 7(d).

Influence of Particle Shape and Size on Magnetic Force (*2*)

The following analysis is based on the assumption that the particles are weakly paramagnetic or diamagnetic.

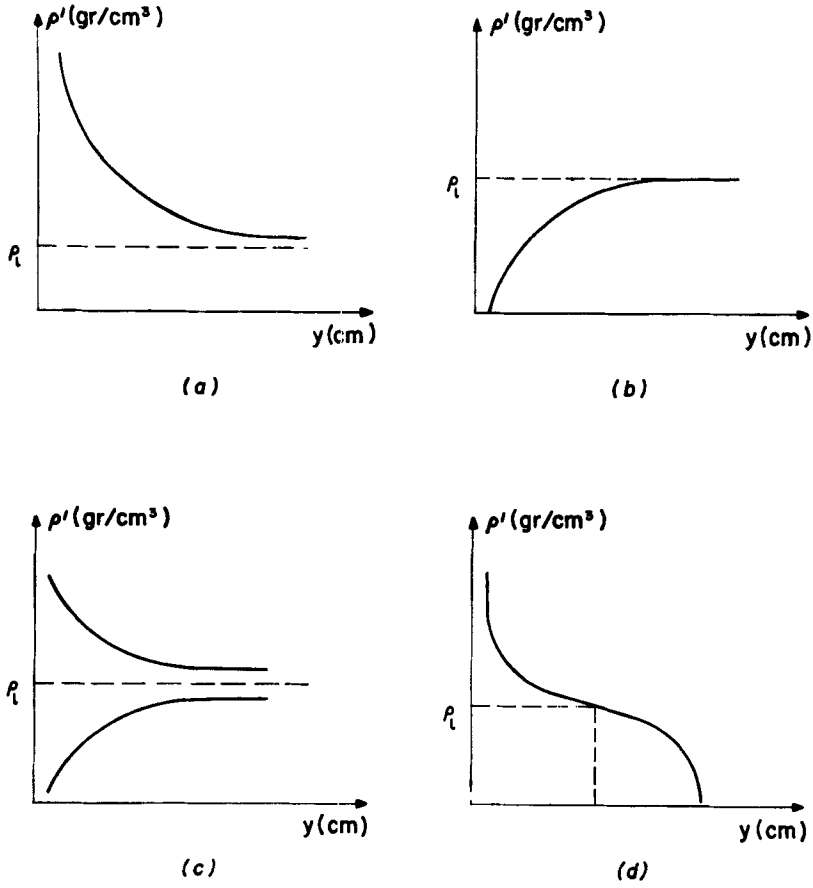

FIG. 7. Distribution of apparent density as a function of y. (a) In weighting of magnetic liquid. (b) In lightening of magnetic liquid. (c) In discontinuous lightening and weighting of magnetic liquid. (d) In continuous lightening and weighting of magnetic liquid.

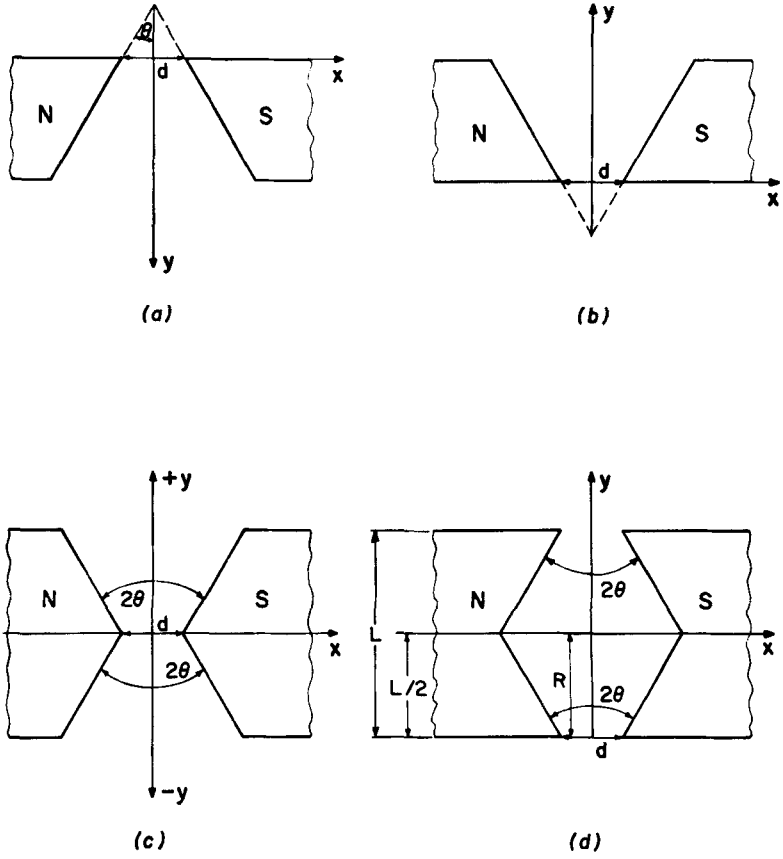

FIG. 8. Pole configuration for the following cases. (a) Lightening the magnetic liquid. (b) Weighting the magnetic liquid. (c) Alternate lightening and weighting of magnetic liquid. (d) Continuous lightening and weighting of magnetic liquid.

Spherical Particle (Fig. 9a). The magnetic force acting on the particle is given by

$$F_m\mathbf{l}y = -\int_V \frac{(\chi_l - \chi_p)A^2}{r^3}\cos\alpha\, dV \tag{18}$$

A unit volume in spherical coordinates is given by

$$dV = z^2\, dz \sin\theta\, d\theta\, d\phi \tag{19}$$

where $z = OA$ (Fig. 9a) and $0 \leq z \leq R$, and in accordance with the figure we have

$$F_m\mathbf{l}y = -\int_0^R \frac{(\chi_l - \chi_p)A^2(l - z\cos\theta)}{(l^2 + z^2 - 2lz\cos\theta)^2} z^2\, dz \int_0^\pi \sin\theta\, d\theta \int_0^{2\pi} d\phi \tag{20}$$

Solving Eq. (20) (see Appendices I and II), we find

$$F_m\mathbf{l}y = -\pi\frac{(\chi_l - \chi_p)A^2}{2}\left[(b^2 + 1)\ln\frac{1+b}{1-b} - 2b\right] \tag{21}$$

Cylindrical Particle (Fig. 9b). A unit volume in cylindrical coordinaties is given by

$$dV = x\, dx\, d\theta\, dz \tag{22}$$

and in accordance with the figure we have

$$F_m\mathbf{l}y = -\frac{(\chi_l - \chi_p)A^2(l - x\cos\theta)}{(l^2 + x^2 - 2lx\cos\theta)^2}\int_0^R x\, dx \int_0^{2\pi} d\theta \int_0^{2R} dz \tag{23}$$

Solving Eq. (23) (see Appendix III), we find

$$F_m\mathbf{l}y = -2\pi(\chi_l - \chi_p)A^2\left[\frac{3b^3 - b}{(1 - b^2)^2} + b\right] \tag{24}$$

where $b = R/l$.

Cubical Particle (Fig. 9c). In accordance with the figure,

$$F_m\mathbf{l}y = -\frac{(\chi_l - \chi_p)}{(y^2 + R^2)^2}\int_{l-R}^{l+R} dy \int_{-R}^{l+R} dx \int_{-R}^{+R} dz \tag{25}$$

Solving Eq. (25) (see Appendix IV), we find

$$F_m\mathbf{l}y = -2\pi(\chi_l - \chi_p)A^2\left[\frac{b}{1-b}\tan^{-1}\left(\frac{b}{1-b}\right) + \frac{b}{1+b}\tan^{-1}\left(\frac{b}{1+b}\right)\right] \tag{26}$$

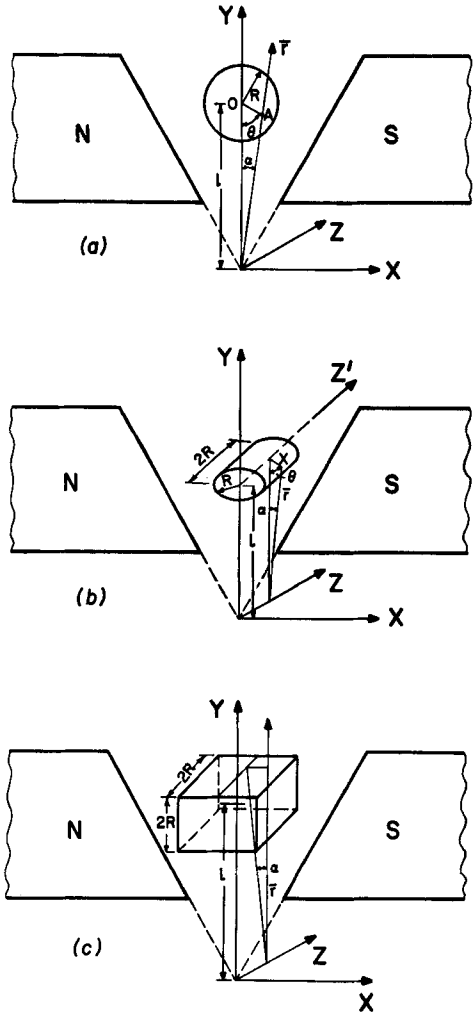

FIG. 9. Coordinates of solid particles in a magnetohydrostatic system. (a) Coordinates of a sphere. (b) Coordinates of a cylinder. (c) Coordinates of a cube.

The influence of particle shape and size on the magnetic force is shown in Tables 1 and 2, clearly indicating that their contribution in stratification of particles with the same density and magnetic susceptibility is minor.

Curved Configuration

In this case the force and field distributions depend on the relevant interval of the parameter k in Eq. (10), as shown in Fig. 10.

For $k > 2$:	Both H and $\nabla\|H\|$ increase with **r**, as does the force.
For $k = 2$:	H increases with **r**, but $\nabla\|H\| = \text{const.}$
For $3/2 < k < 2$:	H increases and $\nabla\|H\|$ decreases with **r**, H being the dominant function. The magnetic force also increases.
For $k = 3/2$:	H increases and $\nabla\|H\|$ decreases with **r** at the same rate, and their product yields $f_m = \text{const.}$
For $1 < k < 3/2$:	H increases and $\nabla\|H\|$ decreases with **r**; $\nabla\|H\|$ being the dominant function, the force decreases.
For $k = 0$:	No force.
For $k = 1$:	$H = \text{const.}$ $\nabla\|H\| = 0$, and the force vanishes.
For $0 < k < 1$:	Both H and $\nabla\|H\|$ decrease with **r**, as does the force.
For $k < 0$:	Both H and $\nabla\|H\|$ decrease with **r**; because of the negative $\nabla\|H\|$, the case is equivalent to a wedge-type configuration with a flatter distribution of the magnetic force.

Selected configurations for some of the above cases are shown in Figs. 11A–11D.

Influence of Spherical Particle Size on Magnetic Force in Curved Configuration (Fig. 12)

According to Eq. (10), the magnetic force acting on a particle in the y-direction is given by

$$F_m|y = (\chi_l - \chi_p)A^2k^2(k-1)\int_V r^{(2k-3)}\cos\alpha\, dV \tag{27}$$

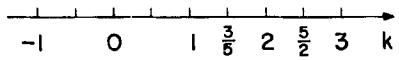

FIG. 10. Interval of k.

TABLE 1

Magnetic Force Values as Function of b for Different Solid Shapes

Shape	Dimensionless magnetic force	$b = 0.05$	$b = 0.1$	$b = 0.15$	$b = 0.20$	$b = 0.25$	$b = 0.30$
Sphere	$F(y)/E^a$	5.22×10^{-4}	4.19×10^{-3}	1.42×10^{-2}	3.39×10^{-2}	6.7×10^{-2}	1.17×10^{-1}
Vertical cylinder	$F(y)/E$	7.88×10^{-4}	6.40×10^{-3}	2.19×10^{-2}	5.33×10^{-2}	10.7×10^{-2}	1.93×10^{-1}
Horizontal cylinder	$F(y)/E$	7.9×10^{-4}	6.40×10^{-3}	2.21×10^{-2}	5.45×10^{-2}	11.1×10^{-2}	2.04×10^{-1}
Cube	$F(y)/E$	10.04×10^{-4}	8.06×10^{-3}	2.77×10^{-2}	6.74×10^{-2}	13.5×10^{-2}	2.42×10^{-1}

[a] $E = (\chi_i - \chi_p)A^2$.

TABLE 2

Location of Particles of Equal Volume and Different Shape in Static Magnetohydrostatic Separation Systems

	$V = 50.93$ cm^3			$V = 33.48$ cm^3			$V = 14.12$ cm^3			$V = 4.18$ cm^3			$V = 2.143$ cm^3			$V = 0.904$ cm^3			$V = 0.267$ cm^3		
Shape	R (cm)	b	l (cm)	R (cm)	b	l (cm)	R (cm)	b	l (cm)	R (cm)	b	l (cm)	R (cm)	b	l (cm)	R (cm)	b	l (cm)	R (cm)	b	l (cm)
Sphere	2.300	0.33	6.96	2.000	0.290	6.90	1.5	0.220	6.80	1.0	0.15	6.66	0.8	0.121	0.60	0.6	0.092	6.52	0.40	0.062	6.45
Cylinder	2.007	0.28	7.142	1.746	0.245	7.07	1.309	0.19	6.88	0.875	0.13	6.715	0.698	0.103	6.64	0.524	0.080	6.55	0.349	0.053	6.48
Cube	1.815	0.20	7.00	1.610	0.232	6.82	1.207	0.178	6.78	0.805	0.121	6.68	0.644	0.097	6.60	0.483	0.074	6.53	0.322	0.049	6.46

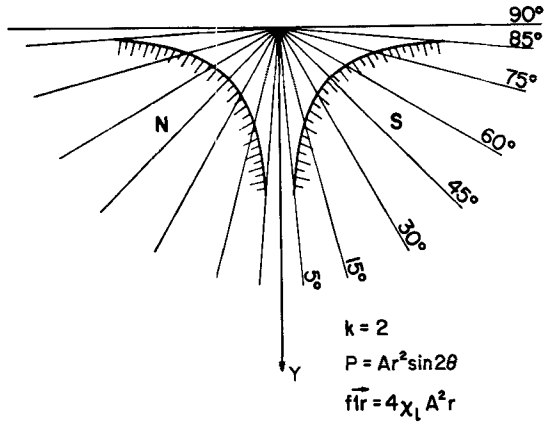

FIG. 11A. Hyperbolic pole configuration in a magnetohydrostatic system.

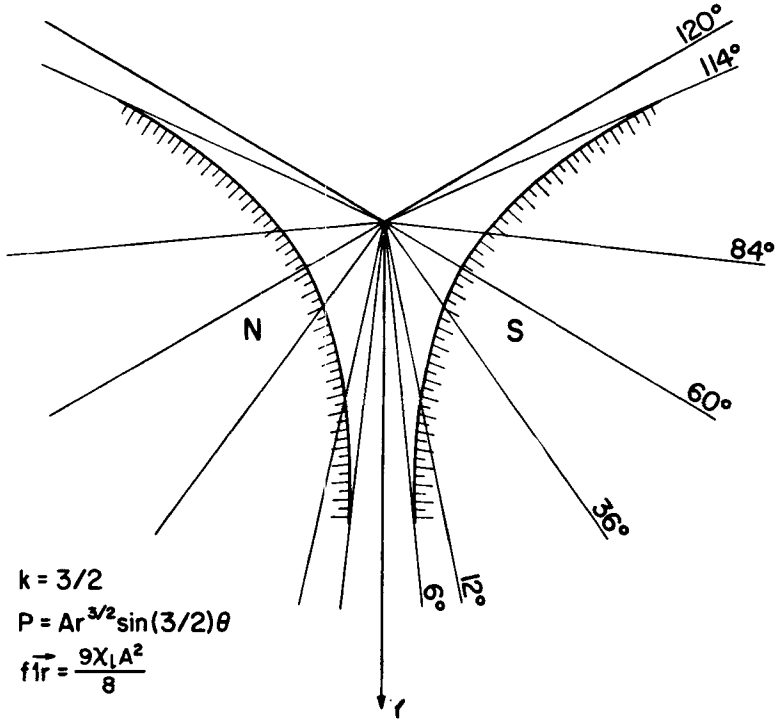

FIG. 11B. Isodynamic pole configuration in a magnetohydrostatic system.

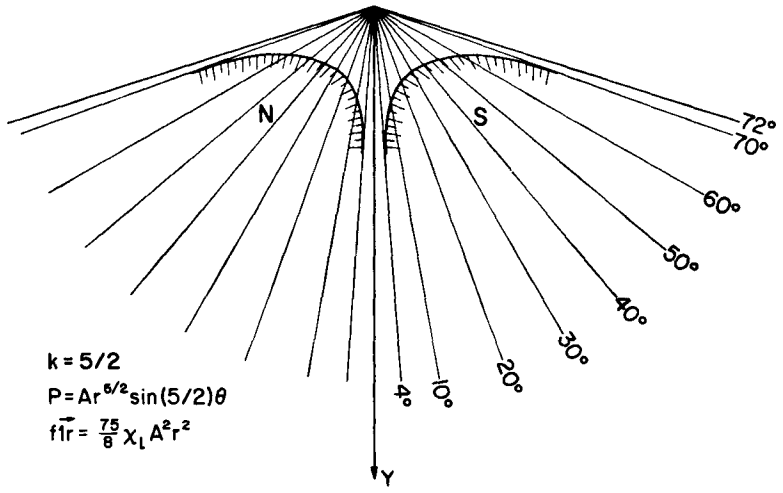

FIG. 11C. Pole configuration for $k = 5/2$ in a magnetohydrostatic system.

Equation (27), in accordance with the geometrical relations in Fig. 12, yields

$$F_m\mathbf{l}y = (\chi_l - \chi_p)A^2k^2(k-1)r^{2(k-2)} \int_0^R x^2\,dx \times \int_0^{2\pi} d\phi \int_0^{\pi} (l - x\cos\theta)\sin\theta\,d\theta \qquad (28)$$

Solving Eq. 28 (see Appendix V), we find

$$F_m\mathbf{l}y = \pi\frac{(\chi_l - \chi_p)A^2k}{2}\left[\frac{(l-R)^{2(k+1)} - (l+R)^{2(k+1)}}{2l^2(k+1)} + \frac{(l+R)^{2k+1} - (l-R)^{2k+1}}{l} + (l-R)^{2k} - (l+R)^{2k}\right] \qquad (29)$$

For $k = 3/2$ (commonly called the isodynamic case), Eq. (29) becomes

$$F_m\mathbf{l}y = 9V\frac{(\chi_l - \chi_p)A^2}{8}\left[1 - \frac{1}{5}\left(\frac{R}{l}\right)^2\right] \qquad (30)$$

It is seen that the behavior is truly isodynamic only when $R/l \to 0$. When R/l is larger, the separator behaves like a screen.

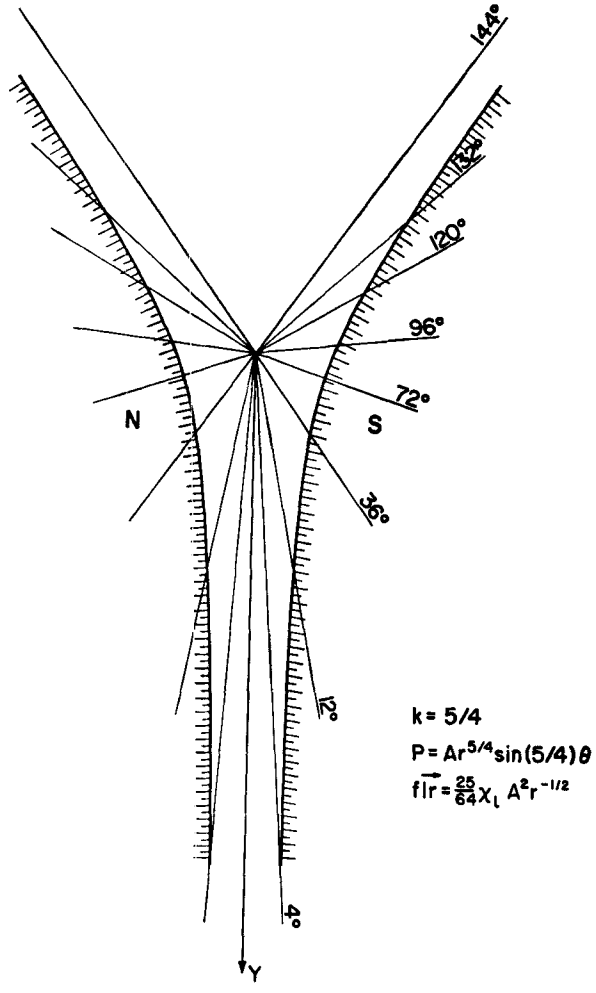

FIG. 11D. Pole configuration for $k = 5/4$ in a magnetohydrostatic system.

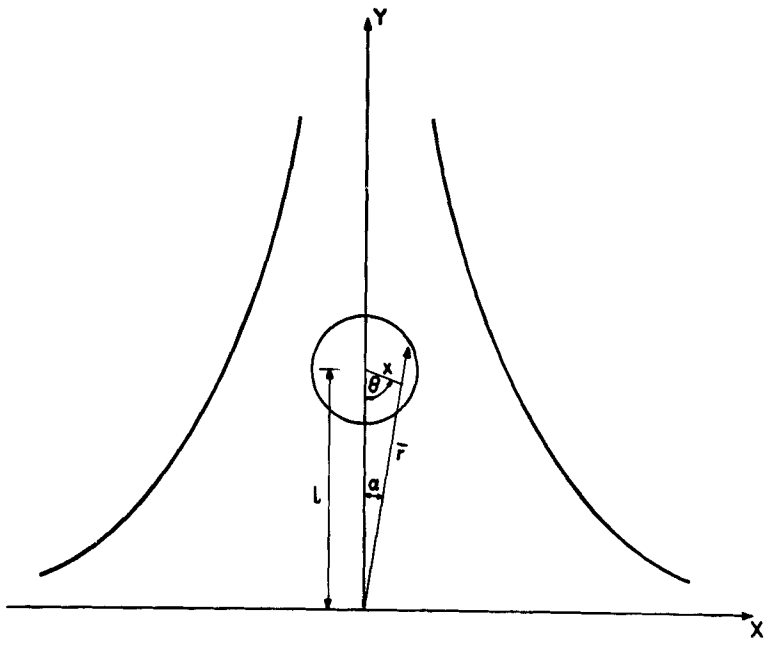

FIG. 12. Spherical particle in curved pole configuration.

EXPERIMENTAL

Measurement of the Magnetic Force Acting on a Spherical Particle

The experiment was carried out on hollow glass spheres (negligible magnetic susceptibility) filled with mercury using a Sartorius mass balance (accuracy $\pm 10^{-4}$ g). See Fig. 13. The variable parameters were the sphere diameter, the air gap, and the applied current. The results in Table 3 (obtained for a magnetic liquid with $\chi_l = 35 \times 10^{-6}$ emu/cm^3) show good agreement between theory and experiment.

Determination of the Magnetic Field Distribution in the *y*-Direction

The experimental device comprised an *x*-*y* recorder and a Bell-G20 gaussmeter. Results for a given air gap and wedge angle are shown in Fig. 14.

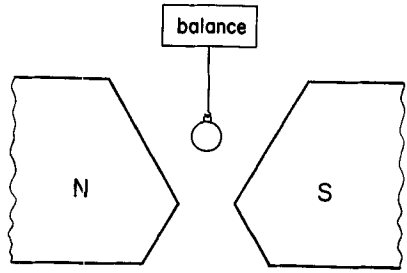

FIG. 13. Measuring device for magnetohydrostatic forces.

TABLE 3

Calculated vs Experimental Force in "Ideal" Zone

Air gap (cm)	l (cm)	R (cm)	b	$A \times 10^{-3}$ Oe·cm	Measured magnetic force F_{mag} (dyn)	Calculated magnetic force F_{mag} (dyn)	ΔF (%)
3.3	6.06	0.89	0.147	20.56	192	197.2	+2.7
	7.65	1.41	0.184	20.56	395	371	−6
	6.06	1.60	0.264	20.56	1085	1161	+7
5.2	10.2	0.89	0.087	20.58	37	39	+5.4
	10.2	1.41	0.138	20.58	165	162	−1.8
	10.2	1.60	0.156	20.58	232	237	+2.1

Influence of Particle Shape on Location

The experiment was carried out with the same balance on particles of uniform size in three shapes. Results are shown in Fig. 15.

Influence of Edge Effects on Magnetic-Force and Magnetic Field Distribution

In order to allow for the edge effect disregarded in the theoretical analysis, the following experimental results are presented in Figs. 16–18.

(a) The magnetic-force distribution as a function of the particle radius, air gap, applied current, and location.
(b) A three-dimensional representation of the isoflux density surface (*4*).

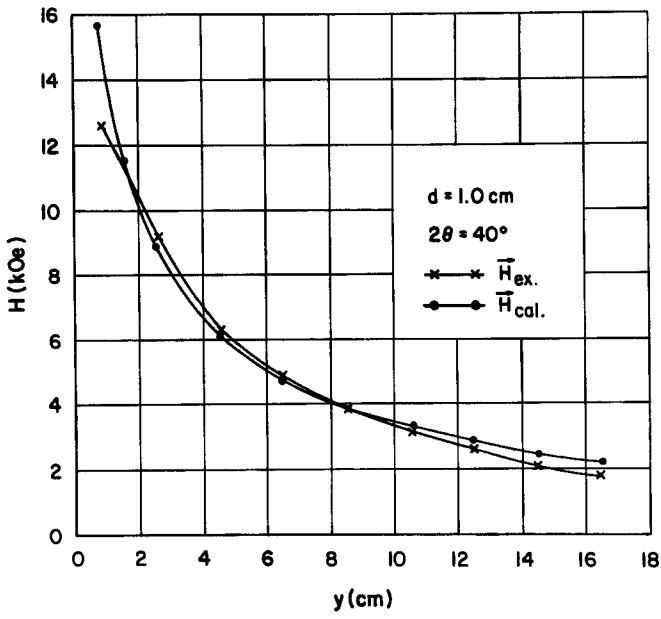

FIG. 14. Magnetic field distribution: calculated vs experimental.

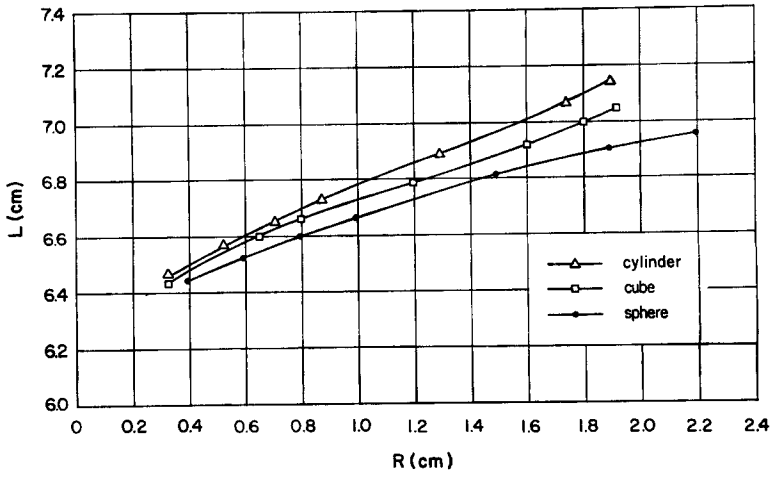

FIG. 15. Influence of particle shape on location in the system.

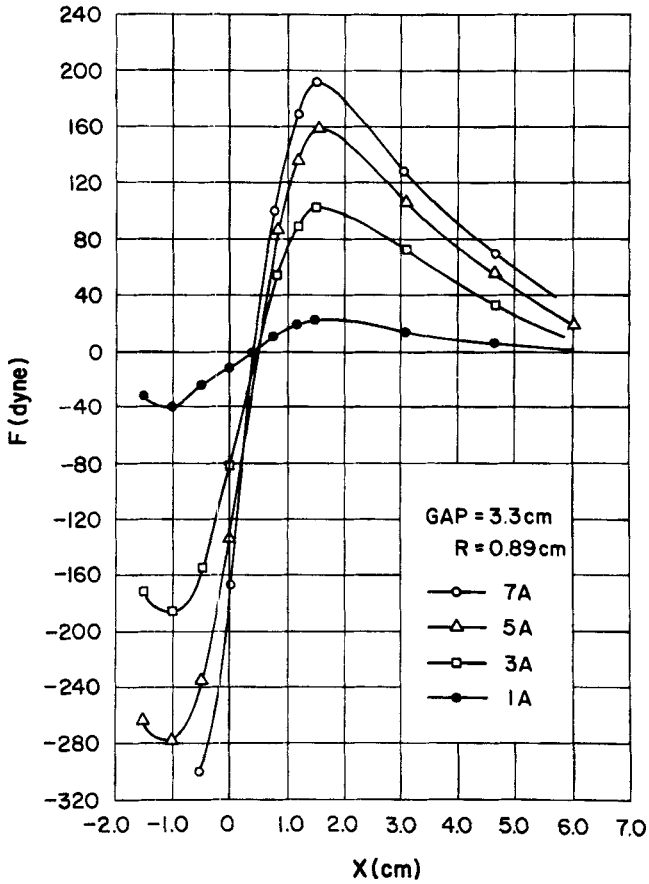

FIG. 16A. Magnetic-force distribution as a function of particle radius, current, and location in the system.

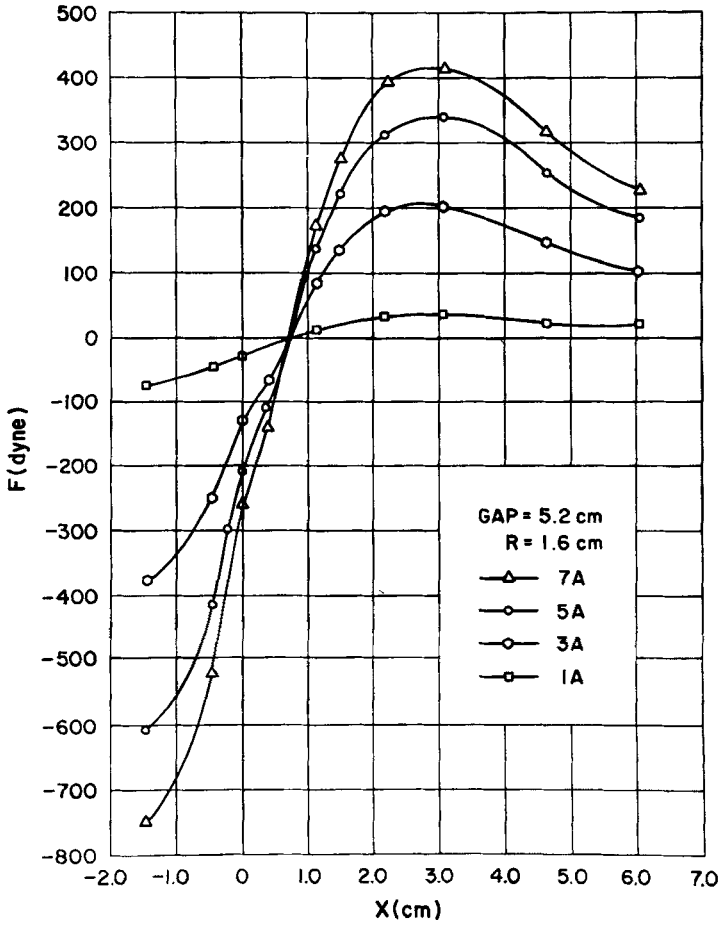

FIG. 16B. Magnetic-force distribution as a function of particle radius, current, and location in the system.

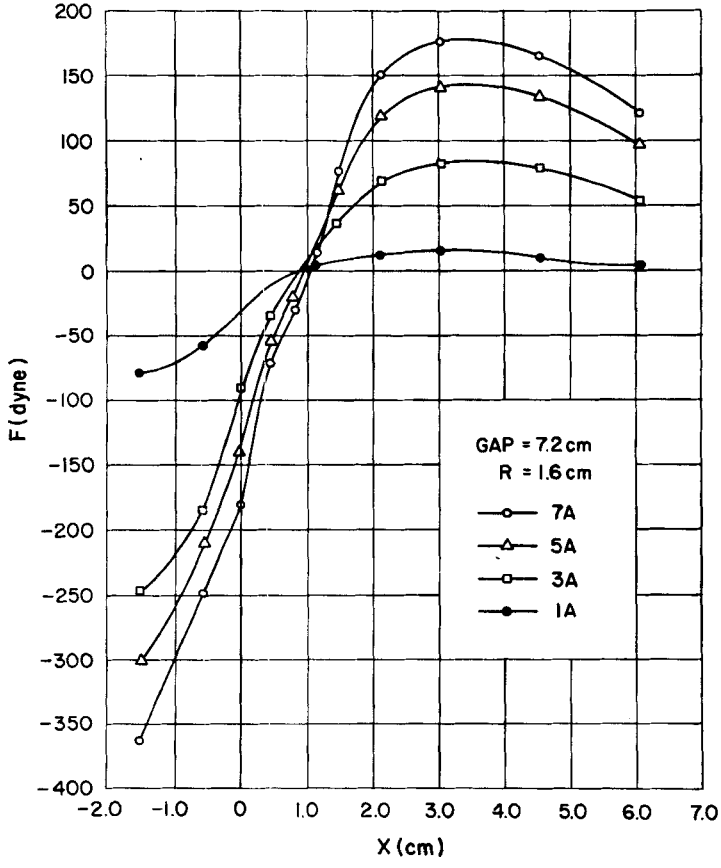

FIG. 16C. Magnetic-force distribution as a function of particle radius, current, and location in the system.

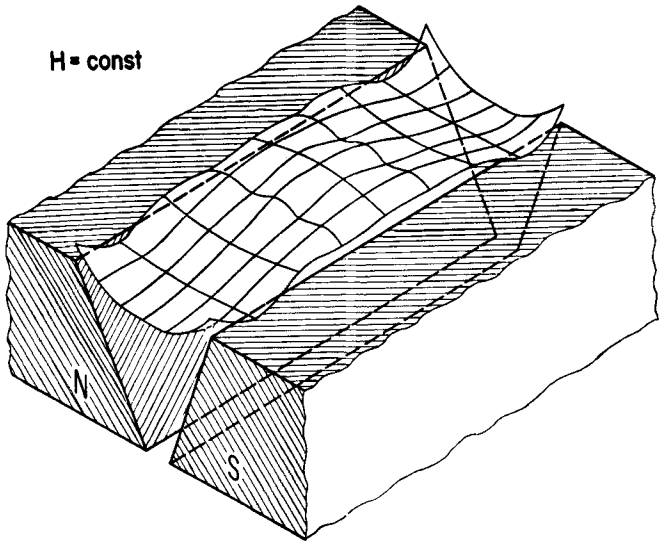

FIG. 17. Three-dimensional representation of the isoflux density surface.

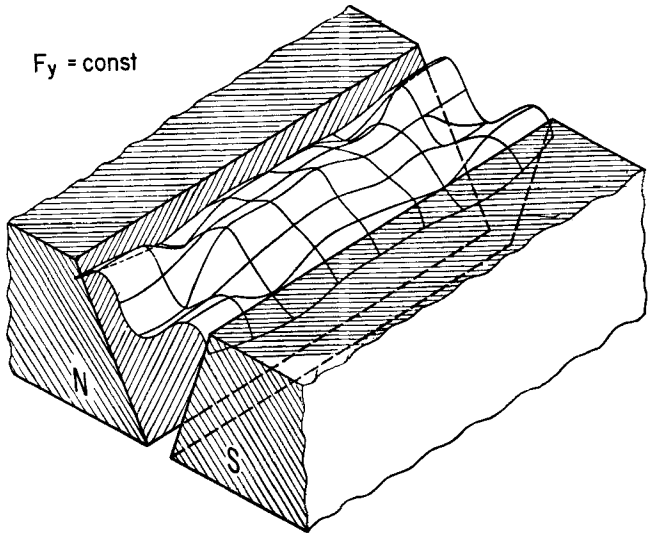

FIG. 18. Three-dimensional representation of vertical isodirectional force.

(c) A three-dimensional representation of the vertical isodirectional force (*4*).

Stratification in Different Pole Configurations (*5*)

The experiment was carried out on three configurations: ordinary wedge-type, wedge-type designed for a negative and positive gradient, and hyperbolic geometry. Results are shown in Fig. 19.

CONCLUSIONS

The following conclusions can be drawn from the results of this work:

(a) The pole configuration can be designed to effect separation of a given mixture of solids, in accordance with their physical properties, on the basis of preliminary calculations.
(b) The stratification pattern of minerals with the same density and magnetic susceptibility is determined by the largest particle size.
(c) The stratification range can be extended by means of a configuration which generates a positive as well as negative field gradient.
(d) Feeding the mixture at half-height of the air gap is recommended, thereby avoiding an edge effect.

The main limitation (*6*) of the method is that the magnetic force can be increased either by reduction of the air gap (whereby the magnetic field is increased) or by use of a high magnetic-susceptibility liquid (e.g., ferrofluid). The first solution curtails the capacity of the separator, the second increases the cost of operation. This problem is currently the object of intensive study at the Mineral Engineering Department of the Technion.

APPENDIX I. SOLUTION OF EQ. (20)

$$F_m\mathbf{l}y = -\int_0^R \frac{(\chi_l - \chi_p)A^2(l - z\cos\theta)}{(l^2 + z^2 - 2lz\cos\theta)^2} z^2\,dz \int_0^\pi \sin\theta\,d\theta \int_0^{2\pi} d\phi$$

Denoting $\alpha = l^2 + z^2$ and $\beta = -2lz$, we have

$$F_m\mathbf{l}y = -2\pi(\chi_l - \chi_p)A^2 \int_0^R z^2\,dz\left[\int_0^\pi \frac{1}{\beta}\left(\frac{l - z\cos\theta}{\alpha + \beta\cos\theta}\right) + \frac{z}{\beta^2}\ln(\alpha + \beta\cos\theta)\right] \quad \text{(I-1)}$$

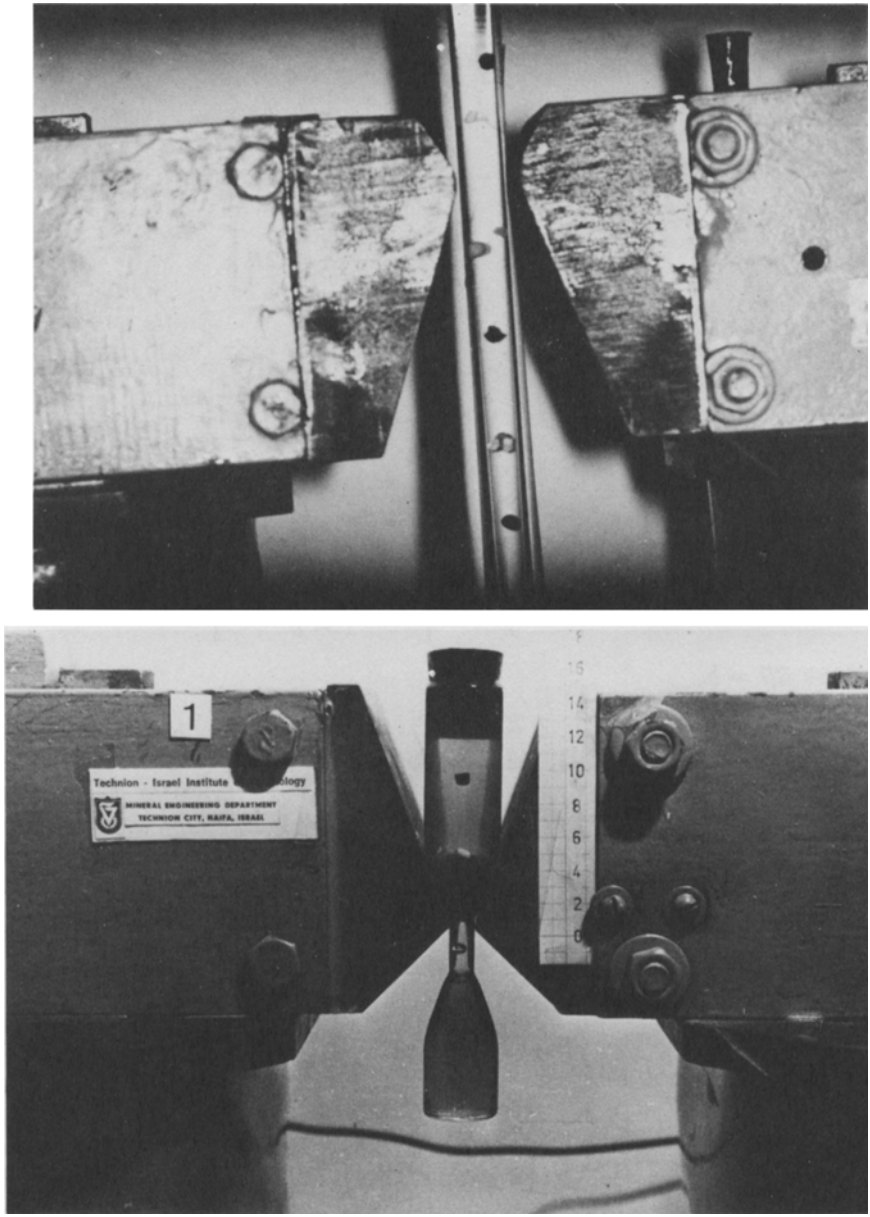

FIG. 19. Mineral stratification in a magnetohydrostatic system in the inverse wedge-type pole configuration (top) and in the wedge-type pole configuration (bottom).

$$F_m\mathbf{l}y = -2\pi(\chi_l - \chi_p)A^2\left[\int_0^R \frac{z^2\,dz}{l(l^2 - z^2)} + \int_0^R \frac{z\,dz}{2l^2}\ln\left(\frac{l+z}{l-z}\right)\right] \quad \text{(I-2)}$$

The first integral equals

$$\int_0^R \frac{z^2\,dz}{l(l^2 - z^2)} = -\frac{1}{2l}\left[l\ln\frac{l-z}{l+z} + 2z\right]_0^R$$
$$= -\frac{1}{2l}\left[l\ln\frac{l-R}{l+R} + 2R\right] \quad \text{(I-3)}$$

and the second equals

$$\int_0^R \frac{z}{2l^2}\ln\left(\frac{l+z}{l-z}\right)dz = \left[\frac{1}{4}\left(\frac{z^2}{l^2} - 1\right)\ln\frac{l+z}{l-z} + \frac{z}{2l}\right]_0^R$$
$$= \frac{1}{4}\left(\frac{R^2}{l^2} - 1\right)\ln\frac{l+R}{l-R} + \frac{R}{2l} \quad \text{(I-4)}$$

whence

$$F_m\mathbf{l}y = -\frac{\pi(\chi_l - \chi_p)A^2}{2}\left[b^2\ln\frac{1+b}{1-b} - 2b\right] \quad \text{(I-5)}$$

where $R/l = b$.

APPENDIX II. VERIFICATION OF EQ. (21)

$$F_m\mathbf{l}y = -\frac{\pi(\chi_l - \chi_p)A^2}{2}\left[b^2\ln\frac{1+b}{1-b} + \ln\frac{1+b}{1-b} - 2b\right]$$

For $b \ll 1$, the logarithmic expression reduces to

$$F_m\mathbf{l}y = -\frac{\pi(\chi_l - \chi_p)A^2}{2}\left[\frac{8b^3}{3} + \frac{2b^5}{3}\right] \quad \text{(II-1)}$$

or, neglecting the highest power of b,

$$F_m\mathbf{l} = -\frac{4\pi b^3}{3}(\chi_l - \chi_p)A^2 \quad \text{(II-2)}$$

Noting that $V = 4\pi R^3/3$, we divide both sides by it and obtain the magnetic force per unit volume:

$$F_m\mathbf{l}y/V = 1(\chi_l - \chi_p)A^2/l^3 \quad \text{(II-3)}$$

APPENDIX III. SOLUTION OF EQ. (23)

$$F_m\mathbf{l}y = -\frac{(\chi_l - \chi_p)A^2(l - x\cos\theta)}{(l^2 + x^2 - 2lx\cos\theta)^2}\int_0^R x\,dx\int_0^{2\pi} d\theta\int_0^{2R} dz$$

Integration with respect to z yields

$$\int_0^{2R} dz = 2R \tag{III-1}$$

and with respect to θ:

$$\int_0^{2\pi}\frac{(l - x\cos\theta)\,d\theta}{(l^2 + x^2 - 2lx\cos\theta)} = \frac{2\pi l(l^2 + x^2)}{(l^2 - x^2)^3} + \frac{4\pi lx^2}{(l^2 - x^2)^3} \tag{III-2}$$

whence

$$F_m\mathbf{l} = -4(\chi_l - \chi_p)A^2R\int_0^R \frac{xl^3 + 3lx^3}{(l^2 - x^2)^3}\,dx \tag{III-3}$$

Finally, substituting $R/l = b$, we have

$$F_m\mathbf{l}y = -2\pi(\chi_l - \chi_p)A^2\left[\frac{3b^3 - b}{(1 - b^2)^2} + b\right] \tag{III-4}$$

APPENDIX IV. SOLUTION OF EQ. (25)

$$F_m\mathbf{l}y = -\frac{(\chi_l - \chi_p)}{(y^2 + x^2)^2}\int_{l-R}^{l+R} dy\int_{-R}^{+R} dx\int_{-R}^{+R} dz$$

As in the preceding case, integration with respect to z yields

$$\int_{-R}^{+R} dz = 2R \tag{IV-1}$$

and with respect to y:

$$\int_{l-R}^{l+R}\frac{y\,dy}{(y^2 + x^2)^2} = \int_{l+R}^{l-R}\frac{1}{y^2 + x^2} \tag{IV-2}$$

whence

$$F_m\mathbf{l}y = -(\chi_l - \chi_p)A^2R\int_{-R}^{+R}\left[\frac{1}{(l - R)^2 + x^2} - \frac{1}{(l + R)^2 + x^2}\right]dx \tag{IV-3}$$

The integrals of the two terms equal, respectively,

$$\int_{-R}^{+R} \frac{dx}{(l-R)^2+x^2} = \left[\int_{-R}^{+R} \frac{1}{l-R} \tan^{-1} \frac{x}{l-R}\right] \tag{IV-4}$$

and

$$\int_{-R}^{+R} \frac{dx}{(l+R)^2+x^2} = \left[\int_{-R}^{+R} \frac{1}{l+R} \tan^{-1} \frac{x}{1+R}\right] \tag{IV-5}$$

whence

$$F_m\mathrm{I}y = -2(\chi_l - \chi_p)A^2\left[\frac{b}{1-b} \tan^{-1}\left(\frac{b}{1-b}\right) - \frac{b}{1+b} \tan^{-1}\left(\frac{b}{1+b}\right)\right] \tag{IV-6}$$

APPENDIX V. SOLUTION OF EQ. (28)

$$F_m\mathrm{I}y = (\chi_l - \chi_p)A^2k^2(k-1)r^{2(k-2)} \times \int_0^R x^2\,dx \int_0^{2\pi} d\phi \int_0^{\pi} (l - x\cos\theta)\sin\theta\,d\theta$$

Noting that $r^2 = l^2 + x^2 - 2xl\cos\theta$, we have

$$F_m\mathrm{I}y = (\chi_l - \chi_p)A^2k^2(k-1)\int_0^R x^2\,dx \int_0^{2\pi} d\phi \times \int_0^{\pi} (l^2 + x^2 - 2lx\cos\theta)^{k-2}(l - x\cos\theta)\sin\theta\,d\theta \tag{V-1}$$

Integration with respect to ϕ yields

$$\int_0^{2\pi} d\phi = 2\pi \tag{V-2}$$

and with respect to θ:

$$\int_0^{\pi} (l^2 + x^2 - 2lx\cos\theta)^{k-2}(l - x\cos\theta)\sin\theta\,d\theta = \left[\int_0^{\pi} \frac{(l^2 + x^2 - 2xl\cos\theta)^{k-1}}{2x(k-1)} - \frac{\cos\theta(l^2 + x^2 - 2lx\cos\theta)^{k-1}}{2lk(k-1)} - \frac{(l^2 + x^2 - 2lx\cos\theta)^4}{4l^2xk(k-1)}\right] \tag{V-3}$$

whence

$$F_m|y = \frac{\pi(\chi_l - \chi_p)A^2k}{2}\int_0^R \left[\frac{2kx}{l}(l + x)^{2k-1} - \frac{x}{l^2}(l + x)^{2k} - \frac{2kx}{l}(l - x)^{2k-1} + \frac{x}{l^2}(l - x)^{2k}\right]dx \quad \text{(V-4)}$$

and finally,

$$F_m|y = \frac{\pi(\chi_l - \chi_p)A^2k}{2}\left[\frac{(l - R)^{2(k+1)} - (l + R)^{2(k+1)}}{2l^2(k + 1)} + \frac{(l + R)^{2k+1} - (l - R)^{2k+1}}{l} + (l - R)^{2k} - (l + R)^{2k}\right] \quad \text{(V-5)}$$

SYMBOLS

A, P	constant and magnetic potential, Oe-cm
b	R/l ratio
d	air gap, cm
F_m	magnetic force, dyn
f_m	magnetic force per unit volume, dyn/cm^3
F_g	gravity force, dyn
F	force acting on a particle, dyn
H	magnetic field intensity, Oe
k	numerical index
R	radius of particle, cm
r	radius vector in coordinate system
V	volume, cm^3
χ_l	magnetic susceptibility of liquid, emu/cm^3
χ_p	magnetic susceptibility of particle, emu/cm^3
ρ_p	density, g/cm^3

REFERENCES

1. W. R. Smythe, *Static and Dynamic Electricity*, McGraw-Hill, New York, 1950.
2. I. Yaniv, "Principal Parameters in Magnetohydrostatic Separation, M.Sci. Thesis in Mineral Engineering, February 1976 (in Hebrew, English synopsis).
3. I. Yaniv, Y. Zimmels, U. Andres, and I. J. Lin, *The Influence of Magnetic Pole Configuration on Mineral Stratification in Magnetohydrostatic Separator*, Research Report MERC 76/A/1, January 1975 (in Hebrew).
4. Y. Zimmels and I. Yaniv, "Characterization of Magnetic Forces by Means of Suspended Particles in Paramagnetic Solutions," *IEEE Trans. Mag.*, *MAG-12*(4), 359–368 (July 1976).

5. I. J. Lin and A. Roisenberg, "Multifractionation of Minerals in a Single Operation," in XIII International Mineral Processing Congress, Sao Paulo, 1977, Paper 5, pp. 1–30.
6. I. J. Lin and N. P. Finkelstein, "The Application of MHS Separation to Metallurgical Problems," *J. S. Afr. Inst. Min. Metall.*, pp. 111–112 (October 1975).

Received by editor July 27, 1978